Received: 10 June 2018 | Revised: 31 October 2018 | Accepted: 2 November 2018

DOI: 10.1002/cta.2586

RESEARCH ARTICLE

WILEY

Three-phase step-up/step-down isolated dc-dc converter with wide-range duty cycle for low dc renewable energy sources applications

Robson Mayer[1] | Menaouar Berrehil El Kattel[1] | Sérgio Vidal Garcia Oliveira[1,2]

[1]Santa Catarina State University UDESC, Joinville, Santa Catarina, Brazil

[2]Blumenau Regional University FURB, Blumenau, Santa Catarina, Brazil

Correspondence
Menaouar Berrehil El Kattel, Santa Catarina State University UDESC, Joinville, Santa Catarina, Brazil.
Email: berrehilelkattel@gmail.com

Summary

Renewable sources of low voltage are an important resource in power generation systems. Many provide high output current at low voltage, as the photovoltaic modules and fuel cells systems, therefore, become more popular considering the safety requirements. In this paper, a novel current-fed three-phase dc-dc converter with high-frequency isolation transformer is proposed. This one has the main features as high dc voltage gain, reduced switches count, minimize the volume of the output/input filters, the frequency ripple of the input current and output voltage are three times higher than the switching frequency, best losses distribution and reduced stresses in the circuit. Moreover, it operates with wide-range duty cycle, the soft-start can be used, which allows the input current and the output voltage to be started gradually. Operating with a duty cycle of 1/3 and 2/3, the input current ripple is canceled. The proposed converter is studied qualitatively and quantitatively, being presented the operation principle in continuous and discontinuous conduction mode, dc voltage gain in each operation mode, and the voltage and current stresses for the power components sizing. To validate the operation of the proposed converter, the laboratory design example and experimental results are presented to demonstrate the performance and validate the claims of the converter for wide load variation. Experimental results are presented for a 4-kW prototype, operating in R2 region for continuous conduction mode. Additionally, experimental results in R1 and R3 regions are obtained.

KEYWORDS

coupled inductor, current-fed, high-frequency isolation, step-up / step-down dc-dc converter, three-phase transformer

1 | INTRODUCTION

Global trends focused on sustainability and increasing demand in the commercial, industrial, and residential sectors have gradually stimulated the area of power generation, to increase their sources and to seek cleaner energy and renewable resources. Renewable resources such as solar, wind, geothermal, and biomass are present around the planet allowing their use in a decentralized, remote, continuous, and without worry of exhaustion since they have their regeneration by

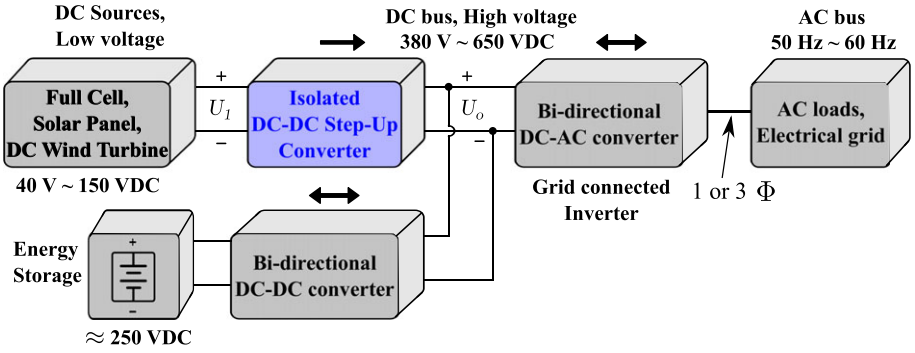

FIGURE 1 Conventional renewable energy power system structure [Colour figure can be viewed at wileyonlinelibrary.com]

natural means. Combination and integration of different sources and energy storage elements in the utility grid allow to obtain a more robust and dynamic electrical system with better performance.[1,2]

Typical energy power system is shown in Figure 1, where the main unidirectional power sources can be derived from a photovoltaic (PV), dc wind, and fuel cells (FC) systems.[1,3,4] In this system, there is a storage element of energy composed of an optional backup battery unit, the dc-dc step-up unidirectional interest stage and a bidirectional dc-ac stage which may be connected to the utility grid or feed alternating current loads. Energy storage systems with batteries have been used and incorporated into the electrical system to supply the energy demands in order to compensate the dynamic characteristics of the sources and fluctuations in energy production, providing an energy reserve when the other sources are not at full capacity.[5-9]

Power electronics is an interface between these power generation and storage systems, integrating with other electrical distribution systems, controlling power flow and operating points, since some of these sources present discontinuous production and are dependent on weather conditions.[10,11] These sources have characteristics such as low output voltage and dependent on the load current, high current with low ripple, respond sluggishly to step changes in load, some having low acceptance to overloads and present highly nonlinear voltage-current characteristics.[12] As a result of these characteristics, and due to the need to regulate the voltage and current in the sources/loads, current-fed dc-dc converters with galvanic isolation are widely applied in the high step-up front-end stage.[13-17]

In Oliveira and Barbi,[18] a three-phase current-fed step-up dc-dc converter with low cost features, high power density and small output filter capacitor has been designed and applied in dc renewable power sources. Do et al[19] propose an isolated single-phase dc-dc converter derived from the classic flyback and use two active switches, two coupled inductors, and four capacitors. In Yang and Do,[20] a high-voltage step-up converter with a single magnetic component is shown, where it provides high dc voltage gain and soft-switching for lower-power application. In Andersen and Barbi,[21] a three-phase push-pull converter with Y-Y transformer connected is tested; however, it has some operating constraints with minimum duty cycle value but is a good candidate to be widely used in fuel cell and photovoltaic applications.[22]

As reported in literatures, several dc-dc converters with a three-phase high frequency (HF) transformer have good efficiency, performance, and some type of active clamp or soft switching technique.[23-27] Additionally, a three-phase transformer provides greater safety and galvanic isolation, high voltage gain, and also increases the filter's operation frequency.[28,29]

This paper aims to provide a complete analysis of the proposed three-phase step-up/step-down dc-dc converter in the three operating regions, continuous, discontinuous, and critical conduction modes. The paper focuses on the detailed analysis of the operation in a wide duty cycle range ($0 \leq D < 1$), providing the full dc voltage gain without a forbidden region and the implementation along with experimental results for continuous conduction mode (CCM). Furthermore, an efficiency of the proposed topology operating in the region R2 using a dissipative resistor-capacitor-diode snubber circuit is showed.

2 | PROPOSED DC-DC CONVERTER

Figure 2 shows the proposed three-phase step-up / step-down dc-dc converter with HF isolation. The current-fed three-phase converter is derived from Andersen and Barbi,[21] where operating restrictions have been solved, new functionalities have been incorporated in the operation with duty cycle less than 1/3, a Y-Delta three-phase transformer provides a higher voltage gain, and input current generated from dc source is continuous, with small ripples.

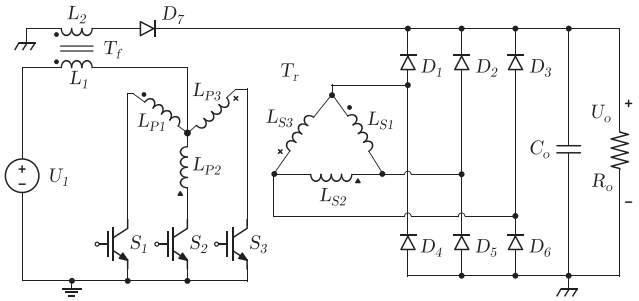

FIGURE 2 Schematic of proposed three-phase dc-dc converter

TABLE 1 Operation regions of the converter

Regions	Duty Cycle	Simultaneity	Superposition
R1	$0 \leq D < 1/3$	1 switch	None
R2	$1/3 \leq D < 2/3$	1 or 2 switches	2 switches
R3	$2/3 \leq D < 1$	2 or 3 switches	3 switches

The three-phase converter is divided into a three-phase full-bridge rectifier configured as six main diodes (D_1–D_6), three main switches (S_1–S_3), and a dc boost inductor L_1 acting as a current source coupled to secondary winding L_2. In general, by adding the secondary winding (L_2) to input inductor and one diode (D_7) connected to output, the converter can operate in the region with duty cycle of 0 to 1/3 (flyback mode), transferring power to output, and simultaneously allow soft-start during the start-up. Furthermore, this circuit provides additional and passive protection to the semiconductors during the occurrence of a drive and control failure or during the protection action for a total shutdown of the drive when it operates at nominal conditions in CCM, transferring the energy stored in the boost inductors to the output. It should be noticed that the three-phase transformer can be given the form of three discrete single-phase transformers connected in Y-Delta winding or a three-legged transformer.

Due to these advantages, this converter is highly recommended as the interface between a low-voltage high-power sources and a succeeding inverter stage. It is also suitable for other low-voltage sources, such as batteries, which supply high-voltage, high-power dc to the next power stages.

The operation regions will be discussed in detail in the following sections for CCM and discontinuous conduction mode (DCM). The proposed topology can be divided into three operating regions, each one depending upon the number of switches in overlapping conditions, according to Table 1.

3 | STEADY-STATE ANALYSIS OF PROPOSED CONVERTER

This section presents the summarized analysis in three operation regions. In CCM, the circuit assumes six operating stages and in DCM assumes nine operating states per switching period. In each of the elements where there is current circulation, the circuit is highlighted. The operating principle of the converter is made considering the following.

To simplify the analysis, the following are assumed over one switching period: (1) The converter is operating in steady-state; (2) the windings of coupled inductor (T_f) and three-phase transformer (T_r) are tightly coupled and have negligible resistance; (3) the output capacitance C_o is large enough to consider a constant output voltage; (4) all semiconductors are ideal.

The pulse width modulation (PWM) switching strategy is used in switches S_1–S_3. The duty cycle D is defined by (1).

$$D = \frac{t_{on}}{T_s}, \tag{1}$$

where t_{on} is the on-time interval of the switches, and T_s is the switching period.

The turns ratio n_L and n_T are defined in (2).

$$n_L = \sqrt{\frac{L_2}{L_1}}; \qquad n_T = \sqrt{\frac{L_{S1}}{L_{P1}}}, \tag{2}$$

where n_L is the turn ratio of the coupled inductor (T_f) and n_T the turn ratio of the three-phase transformer (T_r).

The time intervals of one current period in each stage is shown in Table 2.

3.1 | Operation stages in R1

In region R1, the operation stages for CCM and DCM are presented. The analysis is based on the duty cycle range within 0 to 1/3 , as explained in Table 1. In CCM, the proposed converter has six stages per switching period that can be described as follows.

First stage – $[t_0 \sim t_1]$. Starts when switch S_1 is turned-on, the voltage across the inductor L_1 is $U_1 - U_o/n_T$ and current $i_{L1}(t)$ increases linearly. The load receives energy from the source through diodes D_2 and D_4. Consequently, the currents that flow through S_1 and L_{P1} is the input current. During this stage, L_1 stores energy until t_1 when S_1 is turned-off. This topological stage is shown in Figure 3A.

Second stage – $[t_1 \sim t_2]$. The switch S_1 is turned-off. The energy that has been stored in the inductor L_1 is transferred to the load through the inductor L_2 and the diode D_7. The voltages applied at the terminals of L_1 and S_1 are equal to $-U_o/n_L$ and $U_1 + U_o/n_T + U_o/n_L$, respectively. During this stage, energy is transferred from L_2 to the load through D_7. The equivalent circuit is shown in Figure 3B, which is finalized in t_2 with turned-on of switch S_2.

The second stage also corresponds to the fourth and sixth stages; the equivalent circuit of these stages is similar to the second, as shown in Figure 3B.

Third stage – $[t_2 \sim t_3]$. As shown in Figure 3C, switch S_2 is turned-on, the voltage across the inductor L_1 is $U_1 - U_o/n_T$ and current $i_{L1}(t)$ again increases linearly. The load receives energy from the source through diodes D_3 and D_5. Consequently, the current that flow through S_2 and L_{P2} is the input current. During this stage, L_1 stores energy until t_3, when S_2 is turned-off.

TABLE 2 Time intervals of R1, R2, and R3 in CCM

Regions	First, Third, and Fifth Stages	Second, Fourth, and Sixth Stages
R1	$\Delta t_1 = \Delta t_3 = \Delta t_5 = DT_s$	$\Delta t_2 = \Delta t_4 = \Delta t_6 = (1 - 3D)T_s/3$
R2	$\Delta t_1 = \Delta t_3 = \Delta t_5 = (3D - 1)T_s/3$	$\Delta t_2 = \Delta t_4 = \Delta t_6 = (2 - 3D)T_s/3$
R3	$\Delta t_1 = \Delta t_3 = \Delta t_5 = (3D - 2)T_s/3$	$\Delta t_2 = \Delta t_4 = \Delta t_6 = (1 - D)T_s$

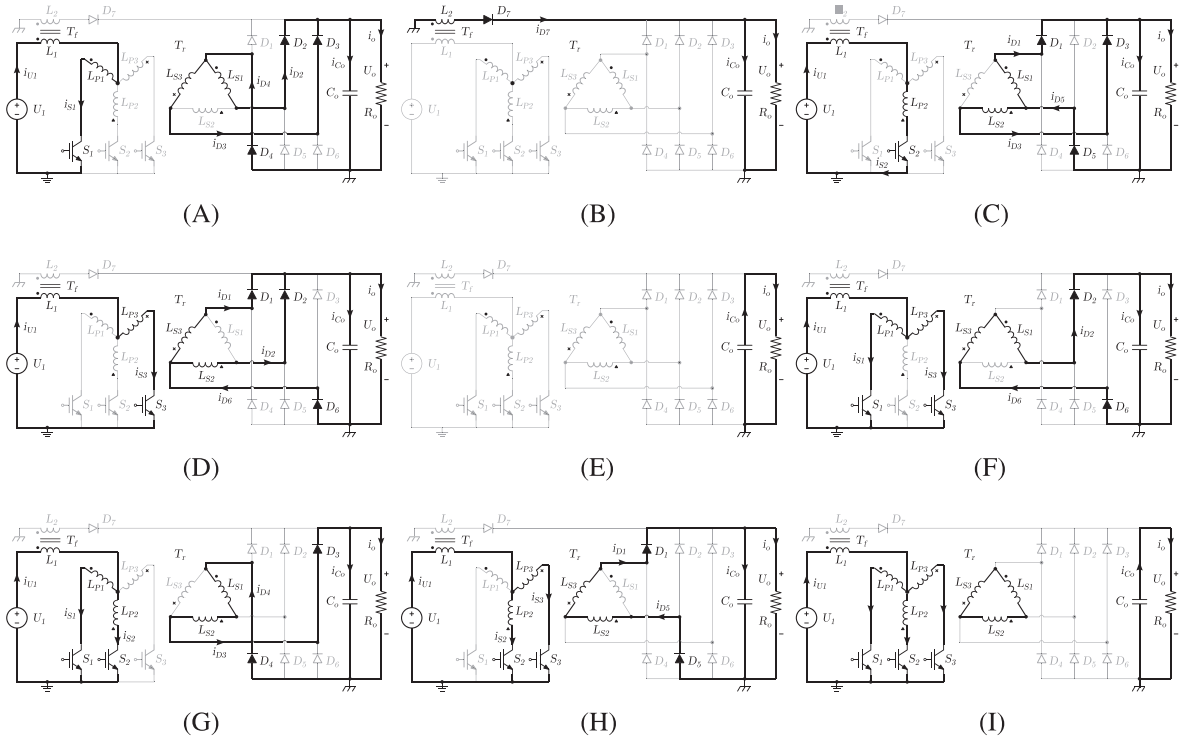

FIGURE 3 Equivalent circuits of operational stages of the proposed topology: A, Stage I in R1, B, Stage II in R1, C, Stage in R1 and R2, D, Stage in R1 and R2, E, Stage in DCM, F, Stage in R2 and R3, G, Stage in R2 and R3, H, Stage in R2 and R3, and I, Stage in R3

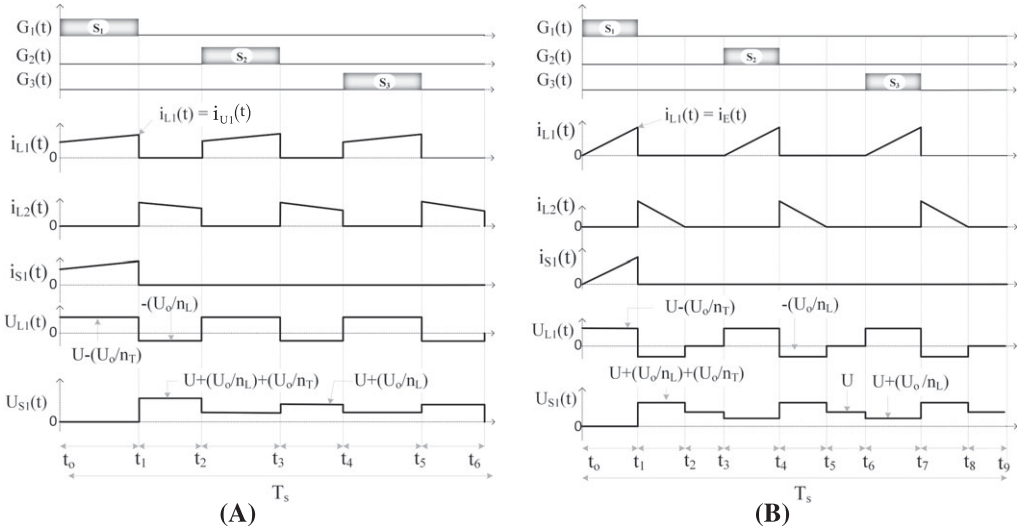

FIGURE 4 Ideal waveforms of the proposed converter in R1: A, for CCM and B, for DCM

Fifth stage – $[t_4 \sim t_5]$. This stage is shown in Figure 3D, starts from t_4, switch S_3 is turned-on, the voltage across the inductor L_1 is $U_1 - U_o/n_T$ and current $i_{L1}(t)$ increases linearly for the third time. The load receives energy from the source through diodes D_1 and D_6. Consequently, the currents that flow through the S_3 and L_{P3} is the input current. During this stage, the L_1 stores energy until t_5, when S_3 is turned-off.

The main voltage and current ideal waveforms for CCM in the different components for a switching period T_s are shown in Figure 4A. The waveforms are obtained from the PWM signals applied in the switches S_1, S_2, and S_3.

In steady state, the average voltage of the primary winding L_1 for the switching period is zero, as given by (3).

$$U_{L1}(t) = \frac{3}{T_s}\left[\int_0^{\Delta t_1}\left(U_1 - \frac{U_o}{n_T}\right)dt + \int_0^{\Delta t_2}\left(-\frac{U_o}{n_L}\right)dt\right] = 0. \tag{3}$$

Substituting the time intervals corresponding to this operating region summarized in Table 2 and the instantaneous voltage of L_1 that correspond to region R1 yields (4).

$$\left(U_1 - \frac{U_o}{n_T}\right)\cdot D - \left(\frac{U_o}{n_L}\right)\cdot\frac{1-3D}{3} = 0. \tag{4}$$

Developing (4), the dc voltage gain in CCM for R1 is given by the following:

$$q_{CCM_{R1}} = \frac{U_o}{U_1} = \frac{3D\cdot n_L\cdot n_T}{3D(n_L - n_T) + n_T}. \tag{5}$$

When the switch S_1 is turned-on, the current through the primary winding of L_1 (coupled inductor T_f) increases, and its voltage is $U_1 - U_o/n_T$. The voltage equation can be given by the following:

$$U_1 - \frac{U_o}{n_T} = L_1\cdot\frac{\Delta I_{U1}}{DT_s}. \tag{6}$$

From (6), the following relation is obtained for the magnetizing inductor or current ripple:

$$\Delta I_{U1} = \Delta I_{L1} = \frac{U_1 - (U_o/n_T)}{L_1}\cdot DT_s. \tag{7}$$

Substituting $U_o = U_1\cdot q_{CCM_{R1}}$ into (7) leads to the input inductance in CCM for R1:

$$L_1 = \frac{U_o}{3n_L\cdot f_s\cdot\Delta I_{U1}}\cdot\overline{\Delta I}_{U1_{R1}}, \tag{8}$$

where the normalized input current ripple is defined by Equation 9.

$$\overline{\Delta I}_{U1_{R1}} = (1 - 3D). \tag{9}$$

In DCM for R1, the proposed converter presents nine stages during a switching period. Therefore, in this operation mode, the inductor current reaches to zero and this occurs in the second, fourth, and sixth stages as shown in Figure 4B and can be described as follows.

First stage – $[t_0 \sim t_1]$. This stage starts at instant t_0, when the transistor S_1 is turned-on and D_4 is reverse biased. The inductor current flows through the three-phase transformer primary winding (L_{P1}) which results in D_2 and D_4 being forward biased. The voltage across the inductor L_1 is $U_1 - U_o/n_T$ and current increases linearly, and therefore, the voltage across L_{P1} is U_o/n_T. Thus, the equivalent circuit of this stage is shown in Figure 3A.

Second stage – $[t_1 \sim t_2]$. This stage starts at instant t_1, when S_1 is turned-off and D_7 is forward biased. The magnitude of the voltage U_{S1} is $U_1 + U_o/n_T + U_o/n_L$, and the energy that has been stored is transferred to the load through the inductor L_2 and the diode D_7. The negative output voltage is applied across to the secondary winding of coupled inductor, and consequently, the induced voltage on the primary winding is $-U_o/n_L$. The equivalent circuit of second stage is shown in Figure 3B, which is finalized in t_2 with turned-on switch S_2.

Third stage – $[t_2 \sim t_3]$. At t_2, all switches are turned-off. The voltage across L_1 is zero. The diodes of the three-phase full bridge rectifier are reverse biased, and only the output capacitor C_o supplies the load. The voltage across the switch S_1 is equal to input voltage. This stage ends at instant t_3 when switch S_2 is turned-on. The third stage corresponds to the sixth and nine stages, as shown in Figure 3E.

The fourth and seventh stages are similar to the first stage, and fifth and eight stages are similar to the second stage. The only difference is that other switches are turned-on.

The dc voltage gain in DCM is determined from the power of the source and the energy consumed by the load. The current waveform shown in Figure 4B, and the average input current during a switching period is given by (10).

$$I_{U1_{avg}} = \frac{3D}{2} \cdot I_{U1_{max}}. \tag{10}$$

The maximum input current ($I_{U1_{max}}$) corresponds to the maximum current value of L_1 ($I_{L1_{pk}} = I_{L1_{max}}$), whose value is calculated by the following:

$$I_{U1_{max}} = \frac{U_1 - (U_o/n_T)}{L_1} \cdot DT_s. \tag{11}$$

Based on principle of energy conversion, that is, the energy supplied by the source is equal to the energy consumed by the load, can be given as follows:

$$U_1 \cdot I_{U1_{avg}} \cdot T_s = U_o \cdot I_o \cdot T_s. \tag{12}$$

Substituting (10) and (11) into (12) yields, the following formula can be given:

$$\frac{2I_o \cdot L_1 \cdot f_s}{U_1} = 3D^2 \left[\frac{U_1}{U_o} - \frac{1}{n_T}\right]. \tag{13}$$

Rearranging and simplifying the expression, the dc voltage gain in DCM can be expressed as follows:

$$q_{DCM_{R1}} = \frac{U_o}{U_1} = \frac{3D^2 \cdot n_T}{n_T \cdot \overline{I_o} + 3D^2}, \tag{14}$$

where the normalized output current can be expressed as follows:

$$\overline{I_o} = \frac{2I_o \cdot L_1 \cdot f_s}{U_1}. \tag{15}$$

The boundary between the CCM and DCM or the critical conduction mode (CrM) is obtained as follows:

$$q_{CCM_{R1}} = q_{DCM_{R1}} \quad \therefore \quad \frac{3D \cdot n_L \cdot n_T}{3D(n_L - n_T) + n_T} = \frac{3D^2 \cdot n_T}{n_T \cdot \overline{I_o} + 3D^2}. \tag{16}$$

From the expression (16), the critical duty cycle D_{Cr} is given by the following:

$$D_{Cr_{R1}} = \frac{1 \pm \sqrt{1 - 12\overline{I_o} \cdot n_L}}{6}. \tag{17}$$

Substituting (17) in (5), one arrives at the following expression for the dc voltage gain at critical conduction.

$$q_{CrM_{R1}} = \frac{(1 \pm \sqrt{1 - 12\overline{I_o} \cdot n_L}) n_T \cdot n_L}{(1 \pm \sqrt{1 - 12\overline{I_o} \cdot n_L})(n_L - n_T) + 2n_T}. \tag{18}$$

3.2 | Operation stages in R2

In this operating mode, the main switches operate with a duty cycle between 1/3 and 2/3 , as explained in Table 1. During each switching period, the converter presents six stages of operation in CCM and the current flowing through the input source is continuous. Therefore, the main waveforms in CCM for region R2 are shown in Figure 5A.

First stage – $[t_0 \sim t_1]$. In this stage (see Figure 3F), beginning from t_0, switches S_1, S_3 are turned-on and switch S_2 is turned-off. The voltage across the primary winding of coupled inductor is $U_1 - U_o/2n_T$, and $i_{L1}(t)$ increases linearly from the initial value. Also, the voltage across L_{P1} is the half of the output voltage reflected to the three-phase transformer primary side $U_o/2n_T$. The load receives energy from the source through secondary windings L_{S1}, L_{S3} and rectifier diodes D_2 and D_6. In this stage, the voltages applied at the terminals of S_1, S_2, and S_3 are equal to 0 V, $3U_o/2n_T$, and 0 V, respectively.

Second stage – $[t_1 \sim t_2]$. In this stage (see Figure 3A), beginning from t_1, switch S_1 keeps turning-on and switches S_2, S_3 are turned-off. The voltage across the primary winding of T_f can be expressed as $U_1 - U_o/n_T$, and hence, $i_{L1}(t)$ decreases linearly. The voltage across L_{p1} can be also expressed as U_o/n_T. The energy is transferred to the load through the rectifier diodes D_2, D_3, D_4 and secondary winding L_{S1}. During this interval, the switch voltages are 0 V, U_o/n_T, and $2U_o/n_T$, respectively.

Third stage – $[t_2 \sim t_3]$. Current flow of the circuit and the state of switches is seen in Figure 3G, where the switches S_1 and S_2 are turned-on and S_3 is turned-off. The voltage across the primary winding of coupled inductor and the three-phase transformer can be obtained as $U_1 - U_o/2n_T$ and $U_o/2n_T$, respectively. During this stage, the primary winding L_1 accumulates energy until the instant t_3, and hence, the current $i_{L1}(t)$ increases linearly. Therefore, the input energy is transferred from the input source to the load through L_{S1}, L_{S2}, D_3, and D_4. The switch voltages are 0 V, 0 V, and $3U_o/2n_T$, respectively.

Fourth stage – $[t_3 \sim t_4]$. At t_3, switch S_2 keeps turning-on and S_1, S_3 are turned-off, as shown in Figure 3C. Thus, the current $i_{L1}(t)$ decreases linearly. The voltage across the primary winding of the coupled inductor and the three-phase transformer can be given as $U_1 - U_o/n_T$ and U_o/n_T, respectively. The energy is transferred from the input source to the load through L_{S2}, D_1, D_3, and D_5. At the end of this stage, the switch voltages across S_1, S_2, and S_3 are $2U_o/n_T$, 0 V, and U_o/n_T, respectively.

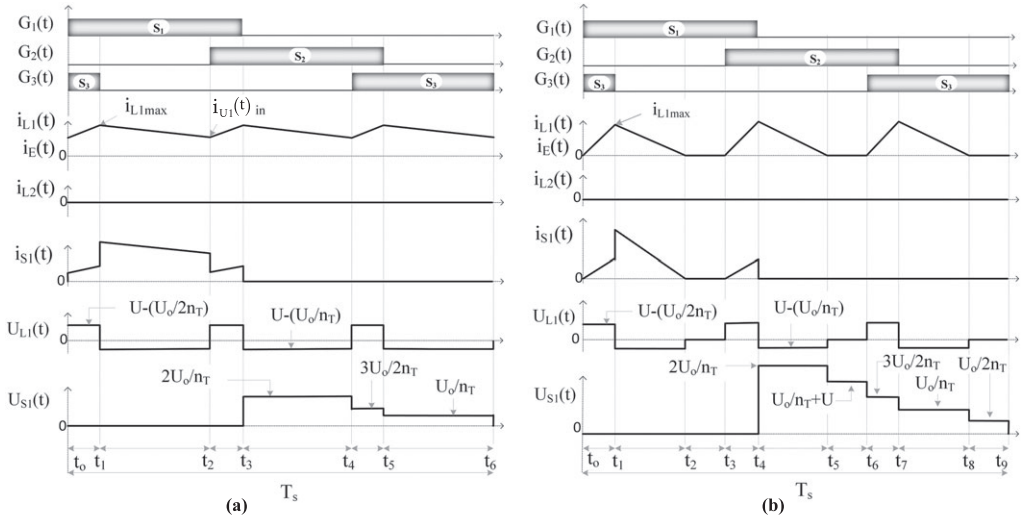

FIGURE 5 Ideal waveforms of the proposed converter in R2: A, for CCM and B, for DCM

Fifth stage – $[t_4 \sim t_5]$. Starts at t_4, when S_3 is turned-on while S_2 is conducting, and hence, the current $i_{L1}(t)$ increases linearly. The voltages across the primary winding of coupled inductor and the three-phase transformer are equal to $U_1 - U_o/2n_T$ and $U_o/2n_T$, respectively. Thus, the load receives energy from the input source through L_{S2}, L_{S3}, D_1, and D_5. The voltage across the switches S_1, S_2, and S_3 are equal to $3U_o/2n_T$, 0 V and 0 V, respectively. This stage ends when S_2 is turned-off at t_5, as shown in Figure 3H.

Sixth stage – $[t_5 \sim t_6]$. During this stage, S_3 keeps turning-on and S_1, S_2 are turned-off. Thus, the current $i_{L1}(t)$ decreases linearly. The input source transfers energy to the load through L_{S2}, L_{S3}, D_1, D_2, and D_6, as illustrated in Figure 3D. Voltage across the primary winding of the coupled inductor and the transformer can be defined as $U_1 - U_o/n_T$ and U_o/n_T, respectively. The reflected output voltage to the primary side of the transformer is applied across switch S_1. Also, the voltages across switches S_2 and S_3 can be represented as $2U_o/n_T$ and 0 V. At t_6, one period of switching operation is ended.

According to the voltage-second balance of primary winding L_1, the dc voltage gain of the proposed converter in CCM for R2 is derived as follows:

$$U_{L1}(t) = \frac{3}{T_s}\left[\int_0^{\Delta t_1}\left(U_1 - \frac{U_o}{2n_T}\right)dt + \int_0^{\Delta t_2}\left(U_1 - \frac{U_o}{n_T}\right)dt\right] = 0. \tag{19}$$

Solving the previous equation applying the time intervals listed in Table 2 for the R2 region, and then rearranging the terms in conveniently form, the dc voltage gain is given by the following:

$$q_{CCM_{R2}} = \frac{U_o}{U_1} = \frac{2}{3}\cdot\frac{n_T}{(1-D)}. \tag{20}$$

The inductance value of coupled inductor should meet the requirement of current ripple, and then it is obtained according to the following expressions:

$$U_{L1}(t) = L_1 \cdot \frac{\Delta I_{L1}}{\Delta t}. \tag{21}$$

From the first stage, see Figure 5A, $\Delta I_{L1} = \Delta I_{U1}$ the inductor voltage (U_{L1}) during the storage stage is given by the following:

$$U_1 - \frac{U_o}{2n_T} = L_1 \cdot \frac{\Delta I_{U1}}{\frac{3D-1}{3}\cdot T_s}. \tag{22}$$

The inductance value of the primary winding of T_f in R2 is obtained as follows:

$$L_1 = \frac{U_o}{6n_T \cdot f_s \cdot \Delta I_{U1}} \cdot \overline{\Delta I}_{U1_{R2}}, \tag{23}$$

where the normalized input current ripple in CCM for R2 is given by the following:

$$\overline{\Delta I}_{U1_{R2}} = (2-3D)\cdot(3D-1). \tag{24}$$

In DCM, the proposed converter presents nine stages during a switching period. As well as in this operation mode, the inductor current reaches to zero and this occurs in the second, fourth, and sixth stages as shown in Figure 5B.

First stage – $[t_0 \sim t_1]$. At t_0, switches S_1, S_3 are turned-on and switch S_2 is turned-off. The equivalent circuit is presented in Figure 3F. The current through the switches S_1, S_3, inductor L_1 and transformer windings L_{P1}, L_{P3} can be represented as follows:

$$I_{S1} = I_{S3} = I_{P1} = I_{P3} = \frac{I_{U1}}{2}; \quad I_{L1} = I_{U1}. \tag{25}$$

Second stage – $[t_1 \sim t_2]$. At t_1, switch S_1 keeps turning-on and switches S_2, S_3 are turned-off; thus, the current in the primary winding of the coupled inductor reaches zero level earlier, even before the end of one-third of a switching period, as shown in Figure 3A. The load receives energy from the source through rectifier diodes D_2, D_3, D_4, and secondary windings L_{S3}, L_{S1}. The currents through the elements are $I_{S1} = I_{U1} = I_{L1} = I_{P1}$.

Third stage – $[t_2 \sim t_3]$. At t_2, the current in the inductor L_1 is equals zero and all diodes of the three-phase bridge rectifier are reverse-biased. Consequently, only the output capacitor C_o feeds the load. This stage ends at the instant t_3, when switch S_2 is turned-on, and thus, the equivalent circuit is shown in Figure 3E.

The fourth and seventh stages are similar to the first stage. The fifth and eighth stages are similar to the second stage and the sixth and ninth stages are similar to the third.

The dc voltage gain in DCM is determined from the energy balance, the supplied by the source and the consumed by load. The energy supplied by the input source during a switching period is given by the following:

$$W_{U1} = 3\,U_1 \cdot \frac{I_{L1_{max}}}{2} \cdot (t_m + t_d) \cdot T_s, \tag{26}$$

where the maximum current of the coupled inductor is a function of the input voltage and the output voltage, the inductance value L_1 is given by the following:

$$I_{L1_{max}} = \frac{U_1 - (U_o/2n_T)}{L_1} \cdot \frac{3D-1}{3} \cdot T_s. \tag{27}$$

The time interval of magnetizing t_m and demagnetizing t_d current is calculated by the following:

$$t_m = \frac{3D-1}{3} \cdot T_s\,; \qquad t_d = \frac{I_{L1_{max}} \cdot L_1}{\frac{U_o}{n_T} - U_1}. \tag{28}$$

Substituting the above expressions (27) and (28) into (26), obtain:

$$W_{U1} = \frac{U_1 \cdot U_o}{2L_1} \cdot \frac{2n_T - q_{DCM_{R2}}}{2n_T} \cdot \frac{(3D-1)^2}{3} \cdot \frac{{T_s}^2}{2(q_{DCM_{R2}} - n_T)}. \tag{29}$$

Applying the energy conversion principle ($W_{U1} = W_o$), it is obtained

$$\frac{2I_o \cdot L_1 \cdot f_s}{U_1} = \frac{2n_T - q_{DCM_{R2}}}{4n_T \cdot (q_{DCM_{R2}} - n_T)} \cdot \frac{(3D-1)^2}{3}. \tag{30}$$

Finally, rearranging (30), the dc voltage gain in R2 for DCM is given by the following:

$$q_{DCM_{R2}} = \frac{U_o}{U_1} = \frac{2n_T \cdot (3D-1)^2 + 12\overline{I_o} \cdot {n_T}^2}{(3D-1)^2 + 12\overline{I_o} \cdot n_T}. \tag{31}$$

The CrM is obtained as follows:

$$q_{CCM_{R2}} = q_{DCM_{R2}} \quad \therefore \quad \frac{2}{3} \cdot \frac{n_T}{(1-D)} = \frac{2n_T \cdot (3D-1)^2 + 12\overline{I_o} \cdot {n_T}^2}{(3D-1)^2 + 12\overline{I_o} \cdot n_T}. \tag{32}$$

Rearranging (32), the critical duty cycle for R2 is given by the following:

$$D_{Cr_{R2}} = \frac{3 \pm \sqrt{1 - 24\overline{I_o} \cdot n_T}}{6}. \tag{33}$$

Substituting (33) in (32) gives (34) which is the dc voltage gain in CrM for R2.

$$q_{CrM_{R2}} = \frac{4n_T}{3 \pm \sqrt{1 - 24\overline{I_o} \cdot n_T}}. \tag{34}$$

3.3 | Operation stages in R3

In each switching period, the converter presents six stages for CCM and nine stages for DCM. These stages are summarized in Table 3. In this operating mode, the duty cycle varies within the range of $2/3 \leq D < 1$, as explained in Table 1.

In region R3, the dc voltage gain of the converter in CCM, DCM, and CrM can be described and summarized by expression (35), when the duty cycle is $D > 2/3$, applying the same principles already used in the previous sections and the time intervals listed in Table 2 for the R3 region.

TABLE 3 Topological stages occurrences in CCM and DCM for R3

Mode	Region R3	
CCM	First stage: Figure 3I	Fourth stage: Figure 3G
	Second stage: Figure 3F	Fifth stage: Figure 3I
	Third stage: Figure 3I	Sixth stage: Figure 3H
DCM	First stage: Figure 3I	Sixth stage: Figure 3E
	Second stage: Figure 3F	Seventh stage: Figure 3I
	Third stage: Figure 3E	Eight stage: Figure 3H
	Fourth stage: Figure 3I	Ninth stage: Figure 3E
	Fifth stage: Figure 3G	

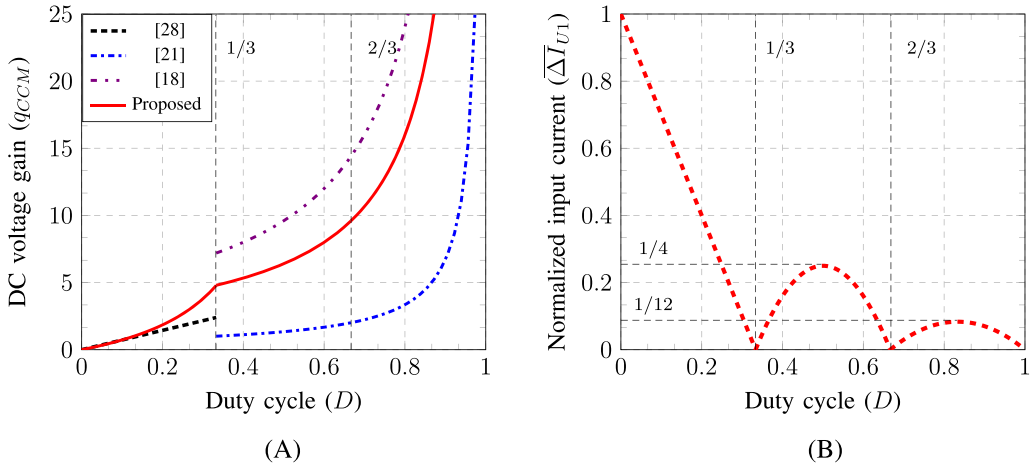

FIGURE 6 Characteristics of the proposed converter in CCM: A, DC voltage gain and B, normalized input ripple current [Colour figure can be viewed at wileyonlinelibrary.com]

$$
\begin{aligned}
q_{CCM_{R3}} &= q_{CCM_{R2}} \\
q_{DCM_{R3}} &= \frac{(3D-2)^2 + 6\overline{I_o} \cdot n_T}{3\overline{I_o}} \\
q_{CrM_{R3}} &= \frac{4n_T}{1 \pm \sqrt{1 - 24\overline{I_o} \cdot n_T}}.
\end{aligned}
\tag{35}
$$

The required inductance value in region R3 is obtained using the above expressions, resulting in the following:

$$
\begin{aligned}
L_1 &= \frac{U_o}{2n_T \cdot f_s \cdot \Delta I_{U1}} \cdot \overline{\Delta I}_{U1_{R3}} \\
\overline{\Delta I}_{U1_{R3}} &= (1-D) \cdot (3D-2).
\end{aligned}
\tag{36}
$$

3.4 | Dc voltage gain, input current ripple, and output characteristics

The expressions (5), (20), and (35) of the proposed converter in CCM can be shown in Figure 6A as a function of the duty cycle for $n_L = 2$, $n_T = 4.8$. Graphically, it can be seen in R2 and R3 the dc voltage gain is similar of basic boost converter circuit, the only difference is the consideration of two-thirds from of three-phase transformer turns ratio. Can be observed that in the region R1, the converter presents a linear dc voltage gain, with characteristic of flyback converter.

The normalized expressions of the input current ripple in (9), (24), and (36) are shown graphically in Figure 6B, where it is noted that for duty cycle of 1/3 and 2/3 result in a complete cancellation of the input current ripple. It is also observed that the maximum input current ripple value in R1 region is $\overline{\Delta I}_{U1} = 1$ for $D = 0$, while in R2 and R3, the maximum value are $\overline{\Delta I}_{U1} = 1/4$ and $\overline{\Delta I}_{U1} = 1/12$ for $D = 1/2$ and $D = 5/6$, respectively. The variation of input current ripple as a function of the duty cycle as proven, and their behavior is similar to the input current ripple of the three-phase dc-dc converters studied in Andersen and Barbi[21] and Larico and Barbi.[28]

The output characteristic of the proposed three-phase converter is illustrated in Figure 7. This graph shows the dc voltage gain for different duty cycle values as a function of normalized output current $\overline{I_o}$. The general plot of Figure 7 can be used for different design parameters, since the normalization is known and can be concluded that when the converter operates with duty cycle equal to 1/3 or 2/3 only CCM operation is obtained. Therefore, the ripple cancellation at the output voltage and the input current occurs for any output load value. This characteristic is of great interest for applications

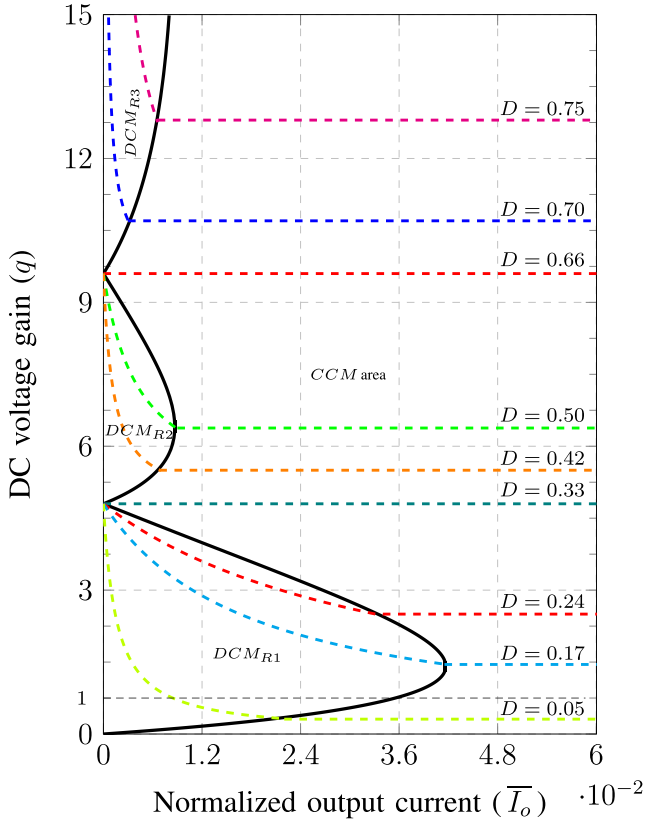

FIGURE 7 Output characteristic of the proposed three-phase converter [Colour figure can be viewed at wileyonlinelibrary.com]

TABLE 4 Device stresses of the proposed three-phase converter

Device	Parameter	Region		
		R1	R2	R3
Inductor	$I_{L1_{avg}}$	$I_o \cdot \frac{3D \cdot n_L \cdot n_T}{3D \cdot (n_L - n_T) + n_T}$	$\frac{2}{3} \cdot I_o \cdot \frac{n_T}{(1-D)}$	
	$I_{L1_{rms}}$	$I_o \cdot \frac{\sqrt{3D} \cdot n_L \cdot n_T}{3D \cdot (n_L - n_T) + n_T}$	$\frac{2}{3} \cdot I_o \cdot \frac{n_T}{(1-D)}$	
	$I_{L2_{avg}}$	$I_o \cdot \frac{n_T \cdot (1-3D)}{3D \cdot (n_L - n_T) + n_T}$	0	
	$I_{L2_{rms}}$	$I_o \cdot \frac{n_T \cdot \sqrt{(1-3D)}}{3D \cdot (n_L - n_T) + n_T}$	0	
Switches	$U_{S_{max}}$	$U_1 + U_o \cdot \left(\frac{1}{n_L} + \frac{1}{n_T}\right)$	$2 \cdot \frac{U_o}{n_T}$	$\frac{3}{2} \cdot \frac{U_o}{n_T}$
	$I_{S_{avg}}$	$I_o \cdot \frac{n_L \cdot n_T \cdot D}{3D \cdot (n_L - n_T) + n_T}$	$\frac{2}{9} \cdot I_o \cdot \frac{n_T}{(1-D)}$	
	$I_{S_{rms}}$	$I_o \cdot \frac{n_L \cdot n_T \cdot \sqrt{D}}{3D \cdot (n_L - n_T) + n_T}$	$\frac{2}{3} \cdot I_o \cdot n_T$	$\frac{\sqrt{2}}{9} I_o \frac{n_T \cdot \sqrt{5-3D}}{(1-D)}$
Bridge rectifier	$U_{D_{max}}$	U_o		
Diodes ($D_1 \sim D_6$)	$I_{D_{avg}}$	$I_o \cdot \frac{n_L \cdot D}{3D \cdot (n_L - n_T) + n_T}$	$\frac{1}{3} \cdot I_o$	
	$I_{D_{rms}}$	$I_o \cdot \frac{n_L \cdot \sqrt{D}}{3D \cdot (n_L - n_T) + n_T}$	$\frac{1}{3\sqrt{3}} \cdot I_o \cdot \frac{\sqrt{7-9D}}{(1-D)}$	$\frac{1}{3} \cdot I_o \cdot \frac{1}{\sqrt{1-D}}$
Diode D_7	$U_{D_{max}}$	$U_o + \left(U_1 - \frac{U_o}{n_T}\right) \cdot n_L$	$U_o + \left(U_1 - \frac{U_o}{2n_T}\right) \cdot n_L$	$U_o + U_1 \cdot n_L$
Capacitor	$I_{C_{rms}}$	$I_o \frac{(n_L - n_T) \cdot \sqrt{3D \cdot (1-3D)}}{3D \cdot (n_L - n_T) + n_T}$	$\frac{1}{3} I_o \frac{\sqrt{(2-3D) \cdot (3D-1)}}{(1-D)}$	$I_o \sqrt{\frac{3D-2}{3 \cdot (1-D)}}$

which do not require voltage regulation, since it reduces the current and voltage ripples providing smaller filter sizes. In R2 and R3 regions, the broadest area in DCM occurs for the duty cycle is 0.5 and 0.83, respectively.

3.5 | Device stresses

Following is performed an analysis of the current and voltage stresses on the active and passive components, whose the converter is analyzed in CCM for R1, R2, and R3 based on the ideal current and voltage waveforms presented. The device stresses are presented assuming that all the parasitic elements are neglected.

The main device stresses of the converter were summarized, and these equations are listed in Table 4.

4 | COMPARISON BETWEEN PROPOSED CONVERTER AND OTHERS THREE-PHASE PUSH-PULL CONVERTERS

In this section, the proposed converter and the main three-phase current-fed push-pull dc-dc converters have been compared. Obtained results compare the components number, operation range of duty cycle, dc voltage gain, active components stress, power rating, peak efficiency and, the most relevant characteristics.

According to Table 5, it can be seen that for duty cycle higher than 1/3, the dc voltage gain of proposed converter is two-third of Andersen and Barbi,[21] and the voltage stress in the R2 region is slightly higher. However, the switch voltage stress is not equal and higher than that of the topology in Larico and Barbi.[28] On the other hand, the switch current stress in the proposed converter is 34 % less than that one proposed in Andersen and Barbi,[21] as can be verified by Table 4, since it reduces the switches conduction losses. Moreover, the three-phase dc-dc topology presented in Andersen and Barbi[21] requires only operation with duty cycle higher than 1/3, and it cannot eliminate the high in-rush current, whereas the proposed converter operates perfectly with full range duty cycle and completely reduces the in-rush current boosting the output voltage gradually without draining high current from the power supply. Finally, the comparison provided in Table 5 reveals that the converter has features for application in high power dc sources and is able to transfer power to the output over wide range duty cycle with reduced stresses.

4.1 | In-rush current limitation

The current-fed type converters such as push-pull is a step-up converter and has a common limitation in which the duty cycle should always be larger than $1/m$ where m is the number of low voltage switches or phases maintaining a path to the boost inductor current.[18,21] Therefore, must always have a switch in the ON state without interruptions of the current in the boost inductors, and in the three-phase converters, this minimum duty cycle will be $1/3$, as well illustrated in Table 5.

This minimum duty cycle limits the control of the output voltage under low-load conditions and causes a very higher in-rush current without a soft-start circuit, resulting in the semiconductors damage, and premature degradation of the power supply.[30,31]

The strategy adopted to solve this limitation is the addition of a secondary winding coupled to the input inductor (L_2), where only one winding is applied on the inductor boost and a simple diode (D_7) is connected to the output of the converter. With this additional circuit, the converter can operate in the region with duty cycle of 0 to 1/3, transferring power to output, and simultaneously allow soft-start during the start-up. Figure 3A,B illustrate and exemplify this operation very well. Furthermore, this circuit provides additional and passive protection to the semiconductors during the occurrence of a drive and control failure or during the protection action for a total shutdown of the drive when it operates at nominal conditions in CCM, transferring the energy stored in the boost inductor to the output.

5 | EXPERIMENT RESULTS

In this section, experimental results are shown for open-loop controller at the CCM in R2 region. Converter analysis, presented in the previous sections and design guidelines that are presented below, is used for this purpose. With the goal of performing tests in both operational regions using the same prototype, other details and more experimental results for R1 and R3 are presented to validate the theoretical analysis in CCM.

The results are obtained for an example system with the specifications given in Table 6. The experimental prototype has been tested under various power conditions.

TABLE 5 Comparison between the three-phase current-fed push-pull converters

Topologies	Oliveira and Barbi[18]	Andersen and Barbi[21]	Larico and Barbi[28]	Larico and Barbi[29]	Proposed
Operation range	$1/3 < D < 1$	$1/3 < D < 1$	$0 \leq D \leq 1/3$	$0 < D < 1$	$0 \leq D < 1$
Counting devices:	3 / 6 / 1 + 3 Inductors,	3 / 6 / 1 + 1 Inductor,	3 / 3 / 1 + 1 Coupled inductor,	3 / 3 / 1 + 1 Coupled inductor,	3 / 7 / 1 + 1 Coupled inductor,
$S/D/C$	1 Y-Y Transformer	1 Y-Y Transformer	1 Y-Y Transformer	1 Y-Y Transformer	1 Y-Δ Transformer
Voltage gain	Forbidden for $D \leq 1/3$	Forbidden for $D \leq 1/3$	$\frac{3n_T \cdot D}{2}$ for $D \leq 1/3$	$\frac{n_T \cdot D}{1-D}$ for $D > 0$	$\frac{3n_L \cdot n_T \cdot D}{3D(n_L - n_T)+n_T}$ for R1
(q_{CCM})	$\frac{n_T}{1-D}$ for $D > 1/3$	$\frac{n_T}{1-D}$ for $D > 1/3$	n / a for $D > 1/3$		$\frac{2n_T}{3(1-D)}$ for R2, R3
Switch voltage	$\frac{U_o}{n_T}$	$\frac{U_o}{n_T}$	$\frac{3U_1}{2}$	$U_1 + \frac{U_o}{n_T}$	$U_1 + \frac{U_o}{n_L}$ for R1
stress					$\frac{2U_o}{n_T}$ for R2
					$\frac{U_o}{n_T}$ for R3
Switch RMS	n / a for R1	n / a for R1	$\frac{I_o n_L n_T \sqrt{D}}{3D(2n_L - n_T)+n_T}$ for R1	n / a for R1	$\frac{I_o n_L n_T \sqrt{D}}{3D(n_L - n_T)+n_T}$ for R1
current	$\frac{I_o n_T \sqrt{2(1-D)}}{2(1-D)}$ for R2	$\frac{I_o n_T}{\sqrt{2(1-D)}}$ for R2	n / a for R2	n / a for R2	$\frac{2I_o n_T}{3}$ for R2
	$\frac{I_o n_T}{3(1-D)}\sqrt{\frac{5-3D}{2}}$ for R3	$\frac{I_o n_T}{3(1-D)}\sqrt{\frac{5-3D}{2}}$ for R3	n / a for R3	n / a for R3	$\frac{I_o n_T \sqrt{2}\sqrt{5-3D}}{9(1-D)}$ for R3
Specification	$U_1 = 48$ V, $U_o = 450$ V,	$U_1 = 120$ V, $U_o = 400$ V,	$U_1 = 120$ V, $U_o = 75$ V,	$U_1 = 100$ V, $U_o = 100$ V,	$U_1 = 75$ V, $U_o = 430$ V,
implemented	$f_s = 20$ kHz, $P_o = 6.8$ kW	$f_s = 40$ kHz, $P_o = 1$ kW	$f_s = 42$ kHz, $P_o = 0.75$ kW	$f_s = 42$ kHz, $P_o = 1$ kW	$f_s = 25$ kHz, $P_o = 4$ kW
Peak efficiency	87 % for 4 kW	94 % for 0.4 kW	93.8 % for 0.56 kW	95.8 % for 0.4 kW	95.0 % for 1.5 kW
				a) Smooth input/output	
Key features	a) High step-up dc	a) Tiny inductance;		ripple current;	a) Step-up and step-down
	voltage gain; b) Higher	b) Higher inrush	a) Circuit simplicity;	b) Absence of the	voltage; b) Full duty
	inrush current for	current for D>1/3;	b) Applications limited	transformer saturation	cycle range operation;
	D>1/3; c) Bulky	c) Forbidden	to low-power; c) Reduced	problem; c) Bulky	c) Allows soft-start
	inductors; d) Suitable	operation region R1;	number of components;	coupled inductor;	function; d) Suitable
	for high-power dc	d) Only step-up	d) High stress in the	d) Very high stress	for high-power low
	sources applications.	operation.	semiconductors.	and leakage problem.	voltage applications.

TABLE 6 Specifications of the experimental prototype

Parameters	Values
Output power	P_o = 0.6kW/4kW/2.4kW; for R1 / R2 / R3
Voltage of input source	U_1 = 75V/75V/40V; for R1 / R2 / R3
Rated output voltage	U_o = 130V/430V/430V; for R1 / R2 / R3
Switching frequency	f_s = 25kHz
Transformer's turns-ratio	n_T = 4.8
Inductor turns-ratio	n_L = 2
Input ripple current	ΔI_{U1} = 4A; to L_1 = 35μH
Output capacitor	C_o = 11μF

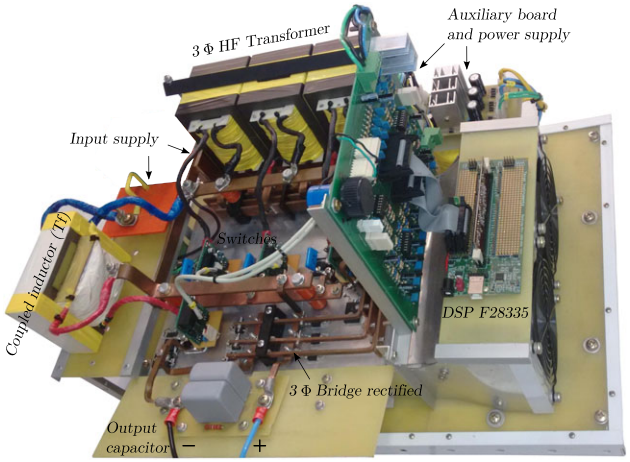

FIGURE 8 Photograph of the laboratory prototype [Colour figure can be viewed at wileyonlinelibrary.com]

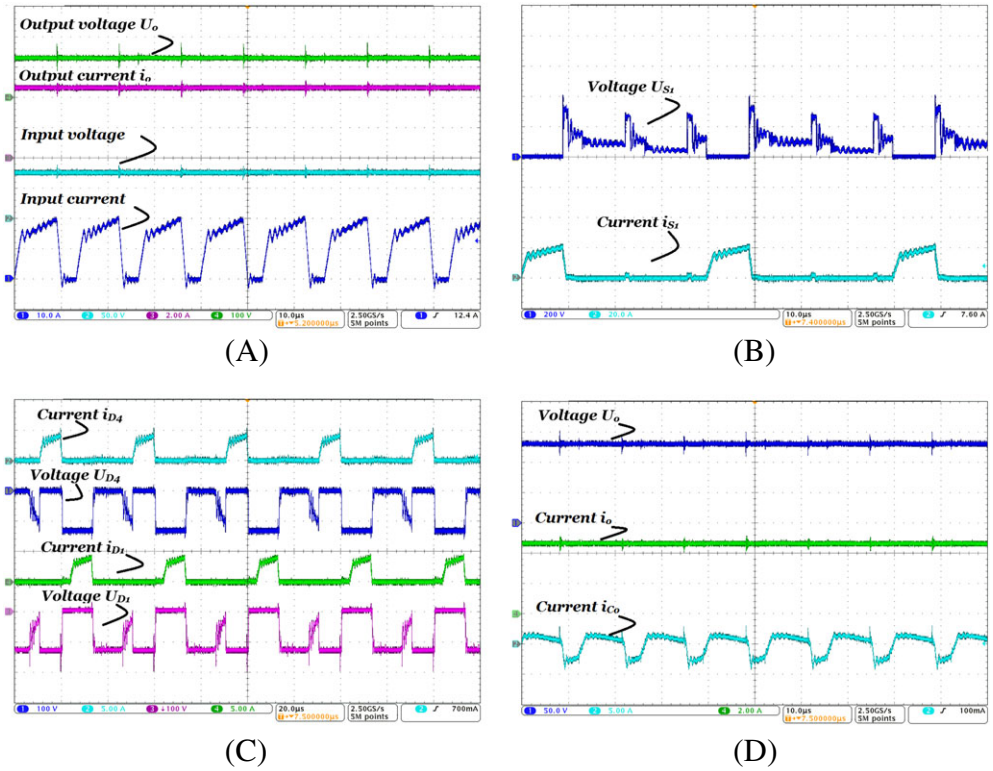

FIGURE 9 Experimental waveforms at R1 for U_1 = 75V, U_o = 130V, D = 0.192: A, Currents and voltages in the load and power supply, B, S_1 switch voltage U_{S1} and current i_{S1}, C, bridge rectifier diodes D_1 and D_4 current i_{D1}, i_{D4} and voltage U_{D1}, U_{D4}, and D, voltage U_o and current i_{Co} of capacitor C_o and output current I_o [Colour figure can be viewed at wileyonlinelibrary.com]

Using the design equations, a 4-kW laboratory prototype is designed to operate as a boost circuit, as shown in Figure 8. The main power components employed were one coupled inductor built in a E core of Kool μ material, three single-phase formers in Y-Δ connection operating as a three-phase HF transformer using ferrite material, two polypropylene output capacitors connected in series with 22 μF / 450 V, and three IGBT switches APT80GP60J. The output rectifier diodes are the APT10SCD120K from Microsemi. Gate signals are generated using TMS320F28335 DSP experimenter kit platform.

The individual snubber circuit containing D_g, R_g, and C_g is used to control the overvoltage across the switches due to the leakage inductances. It was implemented using $R_g = 1.3\text{k}\Omega / 50\text{W}$, $C_g = 0.1\mu\text{F} / 630\text{V}$, and $D_g =$ STTH15S12. The resistor-capacitor-diode (RCD) snubber is designed according to the procedure in Roh et al[32] and Park et al[33] and determined based on the simulation results studies.

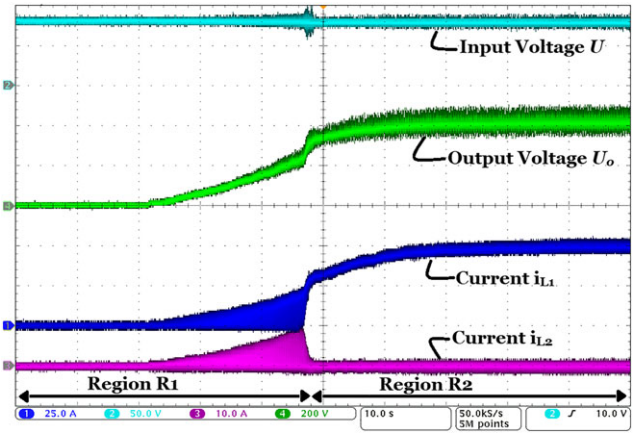

FIGURE 10 Experimental results for operation in R2 using soft-star in region R1 [Colour figure can be viewed at wileyonlinelibrary.com]

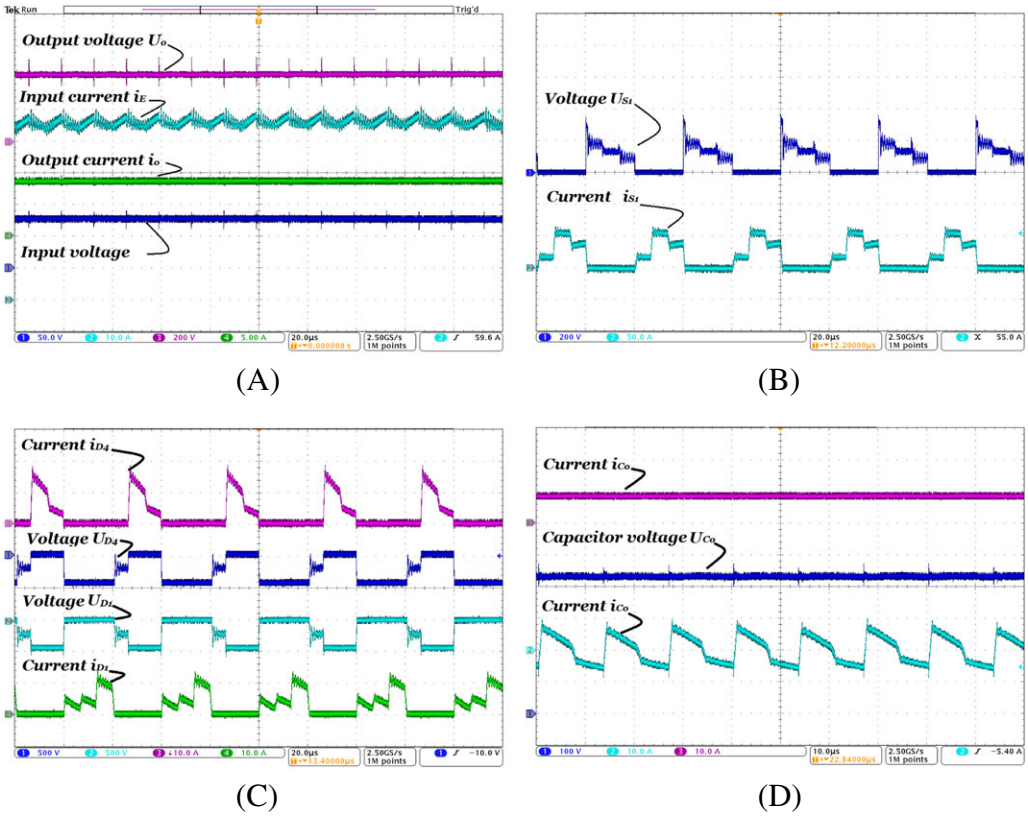

FIGURE 11 Experimental waveforms at R2 for $U_1 = 75\text{V}$, $U_o = 430\text{V}$, $D = 0.442$: A, Currents and voltages in the load and power supply ($I_{U1} = I_{L1}$), B, S_1 switch voltage U_{S1} and current i_{S1}, C, bridge rectifier diodes D_1 and D_4 current i_{D1}, i_{D4} and voltage U_{D1}, U_{D4}, and D, voltage U_o and current i_{Co} of capacitor C_o and output current I_o [Colour figure can be viewed at wileyonlinelibrary.com]

In Figure 9, the experimental waveforms in CCM for R1 are introduced and depicted. The measured results of current and voltage at power supply and at load is shown in Figure 9A. From an input voltage of 75 V, an output voltage of approximately 130 V was obtained, which proves and validates the dc voltage gain in R1, according to the expression (5). Moreover, it can be observed that the input current period is approximately 13 μs, which means the operating frequency is three times higher than the switching frequency, as expected. Figure 9B shows the waveforms on the switch. In the turned-on state i_{S1} is equal to input current and when S_1 is turned-off, the calculated and the experimental result value of U_{S1} is equal to 400 and 170 V, respectively. This voltage difference between the theoretical and experimental result is due to the energy stored in the leakage inductance of three-phase transformer, and the voltage overshoot on the switch is limited by a snubber circuit.

The voltage and current waveforms measured on three-phase rectifier diodes D_1 and D_4 are shown in Figure 9C. The results show the maximum voltage on the diodes is equal to the output voltage, as expected. Figure 9D shows the current and voltage of the output capacitor C_o and the output current. It is noted that the capacitor current frequency also is three times higher than the switching frequency, as expected by theoretical analysis.

Figure 10 shows both the measured output voltage and input current during the soft-start operation. The results show the soft increase of the output voltage and the input current supplied by the low voltage power supply during the transition from R1 to R2 region. The soft-start technique application, the output voltage overshoot and in-rush current are avoided, significantly increasing the source's and converter's lifetime. With the soft-start function is possible to eliminate the in-rush current and start the operation of switches with duty cycle zero and gradually increasing to the rated value.

In Figure 11, the converter's waveforms in CCM for R2 are shown. The current and voltage in the power supply and load can be seen in Figure 11A. From an input voltage of 75 V, an output voltage of approximately 430 V was obtained, which validates the dc voltage gain of the converter for operation in region R2. The input current ripple is approximately 4 A, which is in agreement with the prototype specification in the rated power. Moreover, the input inductor magnetizes and demagnetizes in an interval of approximately 13 μs, which means the operating frequency is three times higher than the switching frequency. The maximum voltage U_{S1} is $2U_o/n_T = 180$ V, as shown in Figure 11B. Diode voltage U_{D1}, U_{D4} and current i_{D1}, i_{D4} at the output three-phase rectifier are shown in Figure 11C. Figure 11D illustrates the current and voltage of the output capacitor C_o, as well as the power consumed by the load.

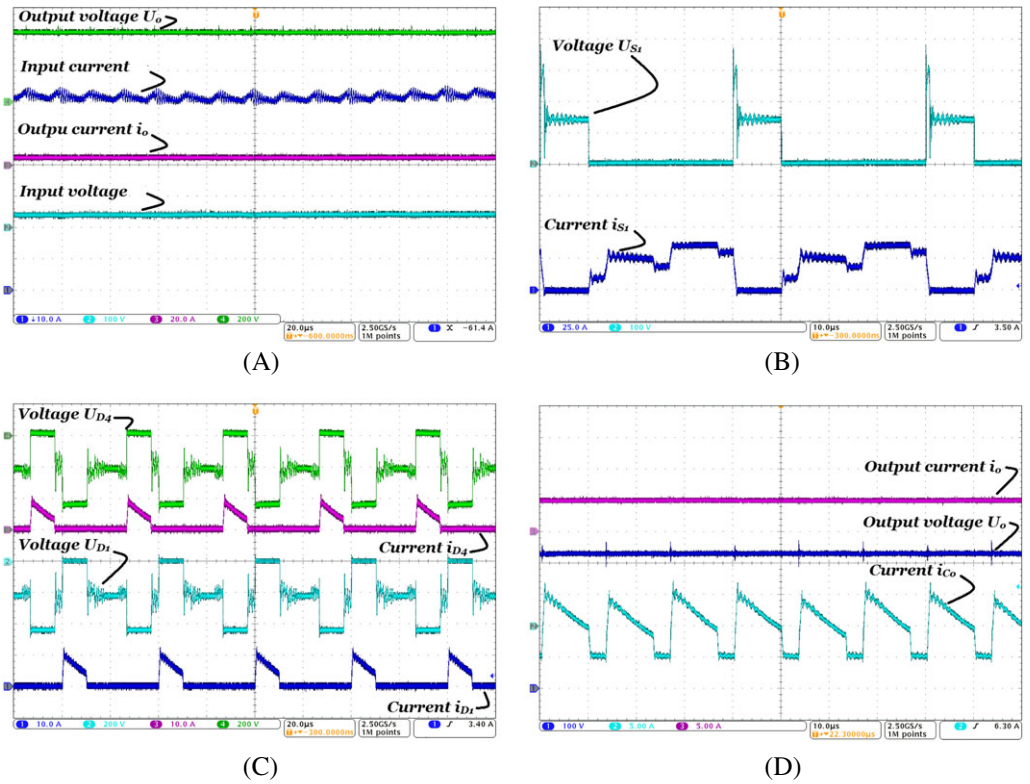

FIGURE 12 Experimental waveforms at R3 for $U_1 = 40$V, $U_o = 430$V, $D = 0.704$: A, Currents and voltages in the load and power supply ($I_{U1} = I_{L1}$), B, S_1 switch voltage U_{S1} and current i_{S1}, C, bridge rectifier diodes D_1 and D_4 current i_{D1}, i_{D4} and voltage U_{D1}, U_{D4}, and D, voltage U_o and current i_{Co} of capacitor C_o and output current I_o [Colour figure can be viewed at wileyonlinelibrary.com]

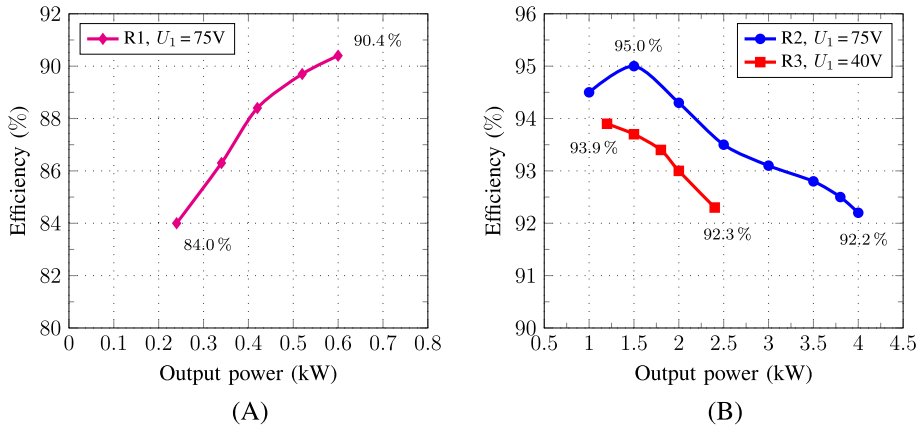

FIGURE 13 Plot of efficiency versus output power for different load conditions: A, In region R1 for output voltage of $U_o = 130$ V and B, in regions R2 and R3, both for output voltage of $U_o = 430$ V [Colour figure can be viewed at wileyonlinelibrary.com]

Figure 12 shows the waveforms for a duty ratio of D = 0.7, ie, the proposed converter is operating in region R3 and CCM. In Figure 12A, is possible to verify the input and the rated output voltage and current. As the converter exhibits a step-up voltage gain, the supply voltage has been reduced to verify for voltage variation at the source and to maintain the same output voltage of the R2 region in the load. Figure 12B,C,D shows the waveforms on the switch, output diodes in the bridge rectifier and the capacitor, respectively. Experimental results match closely with theoretical predicted waveforms and under various electrical conditions.

The converter efficiency was measured for each of the three tested duty cycles in different load conditions in Figure 13. The result of the R1 region is shown in Figure 13A for the proposed current-fed converter. Figure 13B shows measured efficiency for different load conditions at $U_o = 430$V in R2 and R3 regions. The converter's efficiency is close to 96% for the R2 region. The peak experimental efficiency of the proposed converter is obtained as 95% for 1.5 kW, and the full-load efficiency is 92.2%. The obtained efficiency for the converter operating at region R2 and full load can be considered high, considering its rated power and that it works with hard-switching commutation and a dissipative snubber circuit.

6 | CONCLUSION

A new three-phase dc-dc converter with PWM strategy is introduced in this paper, and a 4-kW prototype has been built and tested for the low-voltage dc energy sources and high-power applications. The proposed current-fed push-pull converter circuit is successfully implemented and operates with a wide range duty cycle without forbidden regions. The input and output filters are fed by three times the switching frequency, which will reduce their volume and the size of the converter. This topology operates as a step-up/step-down converter when the duty cycle range is from 0 to 1/3 and step-up voltage from duty cycle higher than 1/3, resulting in the possibility to regulate the output voltage gradually from zero to the rated value. A soft-start technique can be implemented by means of the coupled inductor provides additional and passive protection to the semiconductors during the occurrence of a drive and control failure or during the protection action for a total shutdown of the converter. The proposed converter is a good alternative to the three-phase isolated boost converter in high power from a renewable dc sources application. It is promising for applications requiring higher voltage conversion ratio, higher input with low ripple current, has distinct advantages for high power density and permits compact design, low cost, and high efficiency over wide range of load and input voltage.

ORCID

Menaouar Berrehil El Kattel https://orcid.org/0000-0002-2133-9391

REFERENCES

1. Nehrir MH, Wang C, Strunz K, et al. A review of hybrid renewable/alternative energy systems for electric power generation: configurations, control, and applications. *IEEE Trans Sustainable Energy*. 2011;2(4):392-403.
2. Yu X, Starke MR, Tolbert LM, Ozpineci B. Fuel cell power conditioning for electric power applications: a summary. *IET Electr Power Appl*. 2007;1(5):643-656.

3. Adefarati T, Bansal RC. Integration of renewable distributed generators into the distribution system: a review. *IET Renew Power Gener*. 2016;10(7):873-884.
4. Chub A, Husev O, Blinov A, Vinnikov D. Novel isolated power conditioning unit for micro wind turbine applications. *IEEE Trans Ind Electron*. 2017;64(7):5984-5993.
5. Lo K-Y, Chen Y-M, Chang Y-R. Bidirectional single-stage grid-connected inverter for a battery energy storage system. *IEEE Trans Ind Electron*. 2017;64(6):4581-4590.
6. Wang G, Konstantinou G, Townsend CD, et al. A review of power electronics for grid connection of utility-scale battery energy storage systems. *IEEE Trans Sustainable Energy*. 2016;7(4):1778-1790.
7. Bragard M, Soltau N, Thomas S, De Doncker RW. The balance of renewable sources and user demands in grids: power electronics for modular battery energy storage systems. *IEEE Trans Power Electron*. 2010;25(12):3049-3056.
8. Babaei E, Saadatizadeh Z, Chavoshipour Heris P. A new topology for nonisolated multiport zero voltage switching dc-dc converter. *Int J Circuit Theory Appl*. 2018;46(6):1204-1227.
9. Moradisizkoohi H, Milimonfared J, Taheri M, Salehi S. A high step-up half-bridge dc/dc converter with a special coupled inductor for input current ripple cancelation and extended voltage doubler circuit for power conditioning of fuel cell systems. *Int J Circuit Theory Appl*. 2016;44(6):1290-1307.
10. Blaabjerg F, Chen Z, Kjaer SB. Power electronics as efficient interface in dispersed power generation systems. *IEEE Trans Power Electron*. 2004;19(5):1184-1194.
11. Lin B-R, Chu C-W. Hybrid DC–DC converter with high efficiency, wide ZVS range, and less output inductance. *Int J Circuit Theory Appl*. 2016;44(5):996-1011.
12. Dung NA, Hieu PP, Hsieh Y-C, Lin J-Y, Liu Y-C, Chiu H-J. A novel low-loss control strategy for bidirectional DC–DC converter. *Int J Circuit Theory Appl*. 2017;45(11):1801-1813.
13. Cha H, Choi J, Enjeti PN. A three-phase current-fed dc/dc converter with active clamp for low-dc renewable energy sources. *IEEE Trans Power Electron*. 2008;23(6):2784-2793.
14. Xuewei P, Rathore AK. Current-fed soft-switching push–pull front-end converter-based bidirectional inverter for residential photovoltaic power system. *IEEE Trans. Power Electron*. 2014;29(11):6041-6051.
15. Wu Y-E, Huang K-C. A single-switch cascaded high step-up voltage converter with 95% maximum efficiency for renewable energy systems. *Int J Circuit Theory Appl*. 2016;44(7):1385-1399.
16. Hu Y, Cao W, Finney SJ, Xiao W, Zhang F, McLoone SF. New modular structure dc–dc converter without electrolytic capacitors for renewable energy applications. *IEEE Trans Sustainable Energy*. 2014;5(4):1184-1192.
17. Nguyen M-K, Lim Y-C, Choi J-H, Cho G-B. Isolated high step-up dc-dc converter based on quasi-switched-boost network. *IEEE Trans Ind Electron*. 2016;63(12):7553-7562.
18. Oliveira SVG, Barbi I. A three-phase step-up dc–dc converter with a three-phase high-frequency transformer for dc renewable power source applications. *IEEE Trans Ind Electron*. 2011;58(8):3567-3580.
19. Do H-L. Analysis and implementation of a high-efficiency zero-voltage-zero-current-switching DC–DC converter. *Int J Circuit Theory Appl*. 2013;41(9):889-903.
20. Yang J-W, Do H-L. A soft-switching high step-up dc-dc converter with a single magnetic component. *Int J Circuit Theory Appl*. 2014;42(6):620-631.
21. Andersen RL, Barbi I. A three-phase current-fed push–pull DC–DC converter. *IEEE Trans Power Electron*. 2009;24(2):358-368.
22. Larico HRE, Barbi I. Three-phase push–pull dc–dc converter: analysis, design, and experimentation. *IEEE Trans Ind Electron*. 2012;59(12):4629-4636.
23. Prasad AR, Ziogas PD, Manias S. Analysis and design of a three-phase offline dc-dc converter with high-frequency isolation. *IEEE Trans Ind Appl*. 1992;28(4):824-832.
24. de Souza Oliveira D, Barbi I. A three-phase ZVS PWM DC/DC converter with asymmetrical duty cycle for high power applications. *IEEE Trans Power Electron*. 2005;20(2):370-377.
25. Franceschini G, Lorenzani E, Cavatorta M, Bellini A. 3boost: a high-power three-phase step-up full-bridge converter for automotive applications. *IEEE Trans Ind Electron*. 2008;55(1):173-183.
26. Choi J, Cha H, Han B-M. A three-phase interleaved dc-dc converter with active clamp for fuel cells. *IEEE Trans Power Electron*. 2010;25(8):2115-2123.
27. Xuewei P, Prasanna UR, Rathore A. Magnetizing-inductance-assisted extended range soft-switching three-phase AC-link current-fed DC/DC converter for low dc voltage applications. *IEEE Trans Power Electron*. 2013;28(7):3317-3328.
28. Larico HRE, Barbi I. Three-phase weinberg isolated DC–DC converter: analysis, design, and experimentation. *IEEE Trans Ind Electron*. 2012;59(2):888-896.
29. Larico HRE, Barbi I. Three-phase flyback push–pull DC–DC converter: analysis, design, and experimentation. *IEEE Trans Power Electron*. 2013;28(4):1961-1970.
30. Zhu L, Wang K, Lee FC, Lai J-S. New start-up schemes for isolated full-bridge boost converters. *IEEE Trans Power Electron*. 2003;18(4):946-951.
31. Han S-K, Yoon H-K, Moon G-W, Youn M-J, Kim Y-H, Lee K-H. A new active clamping zero-voltage switching PWM current-fed half-bridge converter. *IEEE Trans Power Electron*. 2005;20(6):1271-1279.
32. Roh C-W, Han S-H, Hong S-S, Sakong S-C, Youn M-J. Dual-coupled inductor-fed DC/DC converter for battery drive applications. *IEEE Trans Ind Electron*. 2004;51(3):577-584.

33. Park K-B, Moon G-W, Youn M-J. Two-transformer current-fed converter with a simple auxiliary circuit for a wide duty range. *IEEE Trans Power Electron*. 2011;26(7):1901-1912.

How to cite this article: Mayer R, Berrehil El Kattel M, Vidal Garcia Oliveira S. Three-phase step-up/step-down isolated dc-dc converter with wide-range duty cycle for low dc renewable energy sources applications. *Int J Circ Theor Appl*. 2019;47:275–293. https://doi.org/10.1002/cta.2586